ChemComm

Accepted Manuscript

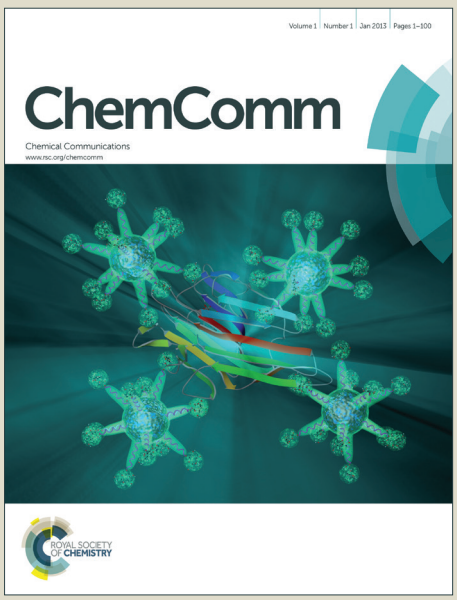

ROYAL SOCIETY OF CHEMISTRY

www.rsc.org/chemcomm

ARTICLE TYPE www.rsc.org/xxxxxx | XXXXXXXX

Co_2N_x/Nitrogen-doped Reduced Graphene Oxide for Enzymeless Glucose Detection

Lingjun Kong, Zhiyu Ren,* Shichao Du, Jun Wu and Honggang Fu*

Received (in XXX, XXX) Xth XXXXXXXXX 200X, Accepted Xth XXXXXXXXX 200X
First published on the web Xth XXXXXXXXX 200X
DOI: 10.1039/b000000x

Co_2N_x/nitrogen-doped reduced graphene oxide (Co_2N_x/NG) are designed and synthesized by electrostatic co-precipitation of Co and rGO followed the high temperature nitridation, which can serve as an efficient catalyst for sensitive glucose detection due to the unique electrocatalytic property of Co_2N_x and synergistic effect between Co_2N_x and N-doped rGO.

Glucose is one of the substance in the life activities which can directly participate in human body's metabolism.[1] Its diagnosis has important significance on the detection of human health and the disease treatment and control.[2] High sensitivity and reliability, fast response and excellent selectivity are of importance to detection, so the electrochemical detection is always concerned on the glucose sensor research.[3] For most electrochemical glucose sensors, the detection is indirect, relying on enzymes.[4] The need for enzyme proteins complicates the sensor construction and compromises the sensitivity, stability, and reproducibility of the sensor due to the poor tolerance to nonphysiological chemical environments and the sensitivity to temperature, pH, humidity, *etc*. So, the non-enzyme glucose determination is attracting people's attention.[5-7] More important, it is essential in the food and chemical diagnoses, bio-processing and the microbial fuel cell.[8, 9]

The traditional non-enzyme glucose sensor is mainly concentrated in noble metal modified electrodes, for example Au, Pt, Pd, *etc*.[10-12] Noble metal has the highest proportion of d-band which is easy to participate in coordination with the carrier or reaction, leading to highly catalytic activity. Despite of that, the high cost is still an unsettling question. Recently, transition metal compounds, such as metal chalcogenide,[13] metal nitride,[14-17] metal carbide,[18] and so on, have shown interesting electrocatalytic properties. In particular, transition metal nitrides, with long durability and environment-friendly character,[19] may be an appealing and low-cost alternative electrochemical catalysts for glucose detection. Nevertheless, the low electron transport efficiency of metal nitrides significantly impedes them from wide use in electrochemical biosensing devices. One of effective strategies to enhance charge transport is to combine metal nitrides with conductive substances,[20, 21] especially for reduced graphene oxide (rGO). Because its abundant defects and chemical groups facilitate charge transfer, resulting in high electrochemical activity.[22-25]

The performance of the hybrid electrode relies on not only the properties of metal nitride and rGO, but also the effective and scalable structure of metal nitride on rGo. The small size and uniform distribution can increase largely the active sites and promote the intimate contact between metal nitride, rGO and glucose, which is important for improving electrocatalytic activity. Generally, the loading of metal nitride on rGO adopts the direct impregnation method, which is difficulty in controlling the size and dispersion of metal nitride.[14, 15] Previously, we synthesized unthin Co nanosheets made up of nanosized clusters, which can be easy assemble with rGO uniformly.[26] More important, as metal precursor, such nanosized Co cluster offers a possible for the fabircation of small-sized cobalt nitrides on rGO.

According to the design, for the first time, Co_2N_x/nitrogen-doped reduced graphene oxide composite (Co_2N_x/NG) is synthesized via two steps. First, the negatively charged Co clusters electrostatic assembled with poly (diallyldimethylammonium chloride) (PDDA)-modified rGO to form Co/rGO. The as-prepared Co/rGO were then converted to Co_2N_x/NG via a consequent nitrided reaction at 500 ºC. The sample, containing 77.70% Co calculated from TG analyses, is denoted as Co_2N_x/NG-500-1 (see experimental section, Table S1 and Fig. S1 in the ESI†). The X-ray diffraction (XRD) analysis (Fig. 1a) indicates that Co nanosheets synchronously transforms into Co_2N and $Co_2N_{0.67}$ during the nitridation at 500 ºC, and then to $Co_{5.47}N$ as the nitridation temperature further increases (Fig. S2). Fig. 2b shows the Raman spectra of Co_2N_x/NG-500-1 and Co_2N_x. Apart from the D-band and G-band peaks at 1350 cm^{-1} and 1580 cm^{-1} of graphitic carbon, four obvious characteristic peaks of Co_2N_x are identified in the spectrum of Co_2N_x/NG-500-1.

Further X-ray photoelectron spectroscopy (XPS) was employed to characterize the surface chemical compositions and valence states of Co_2N_x/NG (Fig. 1c-f). The survey spectra of Co_2N_x/NG-500-1 reveal the presence of C, N, O, and Co in Co_2N_x/NG-500-1 composite. In the Co *2p* XPS of Co_2N_x, two relatively stronger satellite features with respect to $2P_{3/2}$ (780.7 eV) and $2P_{1/2}$ (796.7 eV) confirm the chemical nature of Co^{2+},[27] which is the mainly valence state in electrchemical catalysis.[28, 29] Instead, $Co_{5.47}N$ formed at higher nitridation temperature, will show more metallic chareacter, leading to the inferior performance. To confirm the chemical band of N with Co and C, Co_2N_x in Co_2N_x/NG-500-1 was removed using HCl, denoted as NG. The complex N *1s* XPS of NG can be fitted to three forms: pyridinic-N (398.4 eV), pyrrolic-N (399.6 eV) and pyridinic-N^+O^- (403 eV).[30] Compare to NG, the extra peak at 397.2 eV appears in the high-resolution N *1s* spectra of Co_2N_x/NG-500-1, which is the typical characterstic of metal nitride.[15] These results, in

accordance with our prediction, indicate that not only metal nitrides but also N-doped rGO form via nitrided reaction.

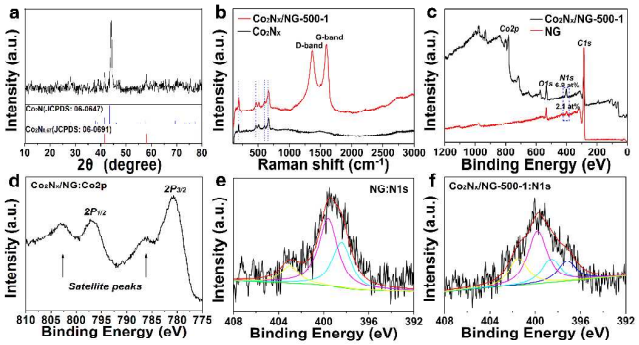

Fig. 1 (a) XRD pattern of Co_2N_x/NG-500-1 and standard XRD patterns of Co_2N and $Co_2N_{0.67}$. (b) Raman spectra of Co_2N_x/NG-500-1 and Co_2N_x. (c) XPS spectra of Co_2N_x/NG-500-1 and NG. (d-f) the high-resolution Co 2p and N 1s XPS spectra of Co_2N_x/NG-500-1 and NG, respectively.

The morphology and structure of Co_2N_x/NG-500-1 composite was examined by TEM, as shown in Fig. 2. NG maintains 2D structure and the distinct folds can be observed. Besides slight aggregation, the sheet-like Co_2N_x with small-sized particles disperses on NG uniformly, illustrating that the nanosized Co clusters can work as metal precursor to control the size of Co_2N_x on rGO. Compared with Co nanosheets and Co/rGO assembly (Fig. S3a-c), the destruction of nanosheets is mainly due to the nitridation reaction. In the case of the absence of rGO, the simple Co_2N_x agglomerates into larger nanoparticles during the high temperature nitriding (Fig. S3d), also implying the firm anchor effects between Co cluster and rGO can restrain the agglomeration of Co_2N_x. So, the BET surface area of Co_2N_x/NG-500-1 (47.3 $m^2 \cdot g^{-1}$) is similar to NG (45 $m^2 \cdot g^{-1}$), which is larger than Co_2N_x (Fig. S4). The corresponding selected area electron diffraction (SAED) clarifies that Co_2N_x are polycrystalline, including Co_2N and $Co_2N_{0.67}$. Indeed, the high-resolution TEM images of Co_2N_x exhibit three lattice spacing corresponding to Co_2N (002) , $Co_2N_{0.67}$ (101), and $Co_2N_{0.67}$ (102) respectively.

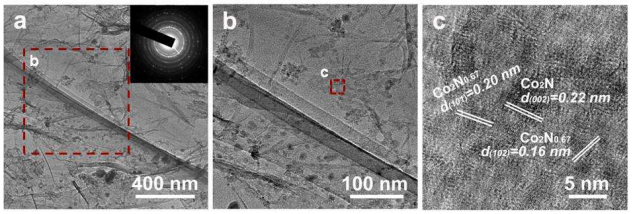

Fig. 2 Typical TEM and HRTEM images of Co_2N_x/NG-500-1, and inset of (a) is the according SAED. The original HRTEM image is shown in Fig. S5.

The electrochemicial performance of the as-synthesized Co_2N_x/NG-500-1 was investigated in a 0.1 M NaOH solution at a scan rate of 50 $mV \cdot s^{-1}$. As shown in the typical cyclic voltammograms (CVs), Co_2N_x/NG-500-1 generates higher redox currents than either Co_2N_x or NG, clarifying that it exhibits the best electrocatalytic activity. The wider redox potentials in CVs of Co_2N_x/NG-500-1 almost involve the charge transfer reactions of Co(II) ↔ Co(III) ↔ Co(IV) in basic electrolyte.[6] Maybe, due to the characteristic of Co_2N_x and the close pontential values, these redox couples tend to overlap with each other. Thus, the electrochemical reaction of Co_2N_x/NG composite might presumably be associated with the redox reaction of Co(II)/Co(IV). With an increase of the scan rate, the reduction current peaks increase (Fig. S6), suggesting a surface-confined electrochemical process. To verify it, electrochemical inpedance spectroscopy (EIS) were investigated, which is an efficient tool for describing the interface properties of modified electrodes. The charge-transfer resistance (R_{ct}) at the electrode surface is equal to the semicircle diameter of EIS at high frequencies. The Nyquist plots reveal that Co_2N_x/NG-500-1 exhibits the smallest R_{ct} as compared to Co_2N_x and NG electrodes (Fig. 2b). The Co_2N_x/NG-500-1 is the most effective in shuttling charges from electrode to glucose, likely due to the excellent catalytic property of Co_2N_x, the intimate contact and synergistic effect between Co_2N_x and NG.[14, 20, 21]

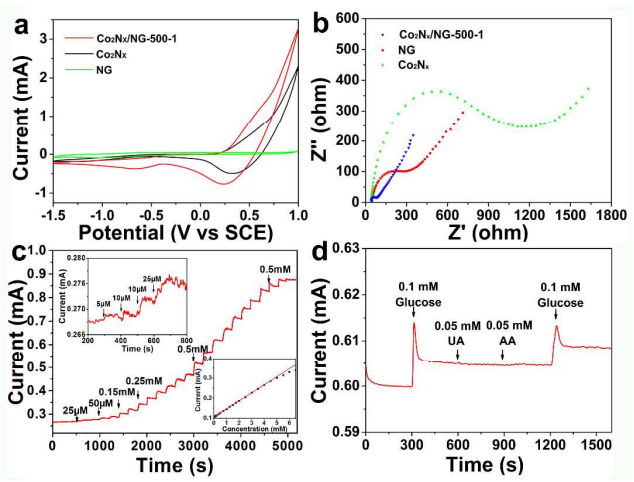

Fig. 3 (a) CVs of Co_2N_x/NG-500-1, Co_2N_x and NG electrodes in 0.1 M NaOH, scan rate: 50 $mV \cdot s^{-1}$. (b) Nyquist plots of Co_2N_x/NG-500-1, Co_2N_x and NG electrodes in 0.1 M KCl containing 2 mM $[Fe(CN)_6]^{3/4-}$. (c) Amperometric response of Co_2N_x/NG-500-1 electrode (holding at 0.25 V vs. SCE) to the successive addition of glucose in 0.1 M NaOH at an applied potential of 0.25 V (vs. SCE). Top inset, a close look of black oval region. Bottom inset, calibration linear relationship of currents *versus* the glucose concentration. (d) Amperometric response to the addition of different analytes to 50 mL of electrolyte (0.1 M NaOH), UA = uric acid, AA = ascorbic acid.

The electrocatalytic activity of Co_2N_x/NG-500-1 electrode to glucose is shown in Fig. S7. The introduction of glucose causes obvious decrease of the reduction current at ~0.25 V, indicating the possible competitive Co(IV) consumption by both Co(II) and glucose.[6] It indicates that Co_2N_x/NG-500-1 exhibits the similar enzyme catalytic activity towards glucose detection.[31] The glucose sensitivity of Co_2N_x/NG-500-1 was evalutated by amperometric measurements at a constant potential of 0.25 V. Fig. 3c shows the typical amperometric response of Co_2N_x/NG-500-1 electrode to the successive addition of glucose into the stirring 0.1 M NaOH with the time interval of 100 s. Each injection of glucose results in an increase of reduction peak current. Obvius response can be observed at addition of 5 μM glucose (the top inset in Fig. 3c), and achieves the maximun steady-state current within 5 s, implying glucose is rapidly obsorbed and activated on the surface of Co_2N_x/NG-500-1. The bottom inset in Fig.3c

depicts a good linear relationship of currents *versus* the glucose concentration in the range of 10 μM to 4.75 mM, and a current plateau is observed when the glucose concentration is higher than 4.75 mM. A linear regression equation of $I\ (mA) = 0.04\ (mA\ mM\text{-}1) \times C\ (mM) + 0.106$, ($n = 3$, $R = 0.994$) is thus derived from the calibration curve, revealing that the glucose sensor has a detection limit as low as 6.93 μM (S/N = 3). The relatively smaller linear range, however, is compensated by the remarkably enhanced sensitivity. Through linear fitting, its sensitivity is up to 1.167 $mA \cdot mM^{-1} \cdot cm^{-2}$, which greatly exceeds those of most previously reported graphene or cobalt oxide/hydroxide-based glucose biosensors (as shown in Table S2). Moreover, the Co_2N_x/NG-500-1 electrode also exhibits excellent selectivity for glucose detection. As shown in Fig. 4d, the addition of interferents, *e.g.*, 0.05 mM of ascorbic acid (AA) and 0.05 mM of uric acid (UA), in 0.1 M NaOH containing 0.1 mM of glucose gives a negligible current changes, while a significant current response is observed for the subsequent addition of 0.1 mM of glucose. Such results, low detection limit, high sensitivity, and high selectivity over interferences, indicate that the as-synthesized Co_2N_x/NG provides a unique possibility of detecting glucose in tear fluid, a relatively simple noninvasive method.[32] In addition, the influence of the nitridation temperature and the Co_2N_x content on the electrocatalytic performance of the as-synthesized Co_2N_x/NG was also investigated (Table S1, Fig. S8 and S9). Evidently, Co_2N_x/NG-500-1 appears the superior electrocatalytic activity and stability.

In summary, Co_2N_x/NG composites were synthetized by the facile two-step produre, including the electrostatic co-precipitation and high temperature nitridation. The small-sized Co_2N_x is attributed to the nanosized Co clusters and the firm anchor effects between Co cluster and rGO. Owing to the advantage of the similar enzyme catalytic activity of Co_2N_x, charge transport property of NG, and synergistic effect between Co_2N_x and NG, the obtained Co_2N_x/NG shows enhanced performances in the limit detection and extraordinary sensitivity of glucose, which provide new insight into the glucose electrochemical biosensors with high sensitivity and stability.

This work was partially supported by the Key Program Projects of the National Natural Science Foundation of China (No. 21031001), the National Natural Science Foundation of China (No. 51102082, 91122018, 21371053), the Cultivation Fund of the Key Scientific and Technical Innovation Project, Ministry of Education of China (No. 708029), Program for Innovative Research Team in University (IRT-1237), Special Research Fund for the Doctoral Program of Higher Education of China (20112301110002), Youth Foundation of Heilongjiang Province of China (QC2013C009).

Notes and references

Key Laboratory of Functional Inorganic Material Chemistry, Ministry of Education of the People's Republic of China; School of Chemistry and Materials Science, Heilongjiang University, 150080 Harbin P. R. China. Fax:+86-451-86661259; Tel: +86-451-86604330; E-mail address: fuhg@vip.sina.com; zyren@hlju.edu.cn.

† Electronic Supplementary Information (ESI) available: Detailed synthetic processes and additional characterizations. See DOI: 10.1039/b000000x/

1 J. Wang, *Chem. Rev.*, 2008, **108**, 814-825.
2 N. J. Ronkainen, H. B. Halsall and W. R. Heineman, *Chem. Soc. Rev.*, 2010, **39**, 1747-1763.
3 M. A. Pleitez, T. Lieblein, A. Bauer, O. Hertzberg, H, V, Lilienfeld-Toal and W. Mäntele, *Anal. Chem.*, 2013, **85**, 1013-1020.
4 B. Q. Zeng, J. S. Cheng, L. H. Tang, X. F. Liu, Y. Z. Liu, J. H. Li and J. H. Jiang, *Adv. Funct. Mater.*, 2010, **20**, 3366-3372.
5 C. T. Hou, Q. Xu, L. N. Yin and X. Y. Hu. *Analyst.*, 2012, **137**, 5803-5808.
6 X.-C. Dong, H. Xu, X.-W. Wang, Y.-X. Huang, M. B. Chan-Park, H. Zhang, L.-H. Wang, W. Huang and P. Chen, *ACS nano.*, 2012, **6**, 3206-3213.
7 X. Wang, X. Dong, Y. Wen, C. Li, Q. Xiong and P. Chen, *Chem. Commum.*, 2012, **48**, 6490-6492.
8 Y. X. Zhao, Z. Y. He and Z. F. Yan. *Analyst.*, 2013, **138**, 559-568.
9 H. Yu, J. Jin, X. Jian, Y. Wang and G. C. Qi, *Electroanalysis.*, 2013, **25(7)**, 1665-1674.
10 Y. Xia, W. Huang, J. F. Zheng, Z. J. Niu and Z. L. Li, *Biosens. Bioelectron.*, 2011, **26**, 3555-3561.
11 C. L. Li, H. J. Wang and Y. Yamauchi, *Chem. Eur. J.*, 2013, **19**, 2242-2246.
12 H. Jansa and Q. Huo, *Chem. Soc. Rev.*, 2012, **41**, 2849-2866.
13 J. Xu, Q. F. Wang, X. W. Wang, Q. Y. Xiang, B. Liang, D. Chen and G. Z. Shen, *ACS nano.*, 2013, **7**, 5453-5462.
14 X. Zhang, X. Chen, K. Zhang, S. Pang, X. Zhou, H. Xu, S. Dong, P. Han, Z. Zhang, C. Zhang and G. Cui, *J. Mater. Chem. A*, 2013, **1**, 3340-3346.
15 L, Wang, J. Yin, L. Zhao, C. G. Tian, P. Yu, J. Q. Wang and H. G. Fu, *Chem. Commun.*, 2013, **49**, 3022-3024.
16 S. M. Wang, X. H. Yu, Z. J. Lin, R. F. Zhang, D. W. He, J. Q. Qin, J. L. Zhu, J. T. Han, L. Wang, H. Mao, J. Z. Zhang and Y. S. Zhao, *Chem. Mater.*, 2012, **24**, 3023-3028.
17 Z. Wen, S. Cui, H. Pu, S. Mao, K. Yu, X. Feng and J. Chen, *Adv. Mater.*, 2011, **23**, 5445-5450.
18 R. H. Wang, C.G. Tian, L. Wang, B. L. Wang, H. B. Zhang and H. G. Fu, *Chem. Commun.*, 2009, 3104-3106.
19 M. I. Kim, Y. J. Ye, B. Y. Won, S. Shin, J. Lee, and H. G. Park, *Adv. Funct. Mater.*, 2011, **21**, 2868-2875.
20 H. L. Wang and H. J. Dai, *Chem. Soc. Rev.*, 2013, **42**, 3088-3113.
21 Y. Y. Liang, Y. G. Li, H. L. Wang and H. J. Dai, *J. Am. Chem. Soc.*, 2013, **135**, 2013-2036.
22 H. L. Wang, Z. W. Xu, A. Kohandehghan, Z. Li, K. Cui, X. H. Tan, T. J. Stephenson, C. K. King'ondu, C. M. B. Holt, B. C. Olsen, J. K. Tak, D. Harfield, A. O. Anyia and D. Mitlin, *ACS nano.*, 2013, **7**, 5131-5141.
23 D. Chen, H. B. Feng and J. H. Li, *Chem. Rev.*, 2012, **112**, 6027-6053.
24 B. Y. Xia, B. Wang, H. B. Wu, Z. L. Liu, X. Wang and X. W. Lou, *J. Mater. Chem.*, 2012, **22**, 16499-16505.
25 G. Q. Zhang, B. Y. Xia, X. Wang and X. W. Lou, *Adv. Mater.,* 2013, DOI: 10.1002/adma.201304683.
26 S. Du, Z. Ren, Y. Qu, J.-Q. Wang, L. Kong, K. Shi, B. H. Bateer and H. Fu, *ChemPlusChem.*, 2013, **78**, 481-485.
27 L. Liao, Q. Zhang, Z. Su, Z. Zhao, Y. Wang, Y. Li, X. Lu, D. Wei, G. Feng, Q. Yu, X. Cai, J. Zhao, Z. Ren, H. Fang, F. Robles-Hernandez, S. Baldelli and J. Bao, *Nat. Nanotech.*, 2014, **9**, 69-73.
28 X.-Y. Lang, H.-Y. Fu, C. Hou, G.-F. Han, P. Yang, Y.-B. Liu and Q. Jiang, 2013, 4, *Nat. Commun.*, 2013, **4**, 2169.
29 Y. Liang, H. Wang, P. Diao, W. Chang, G. Hong, Y. Li, M. Gong, L. Xie, J. Zhou, J. Wang, T. Z. Regier, F. Wei, H. Dai, *J. Am. Chem. Soc.*, 2012, **134**, 15849-15857.
30 Y. Wang, Y.Y. Shao, D. W. Matson, J. H. Li and Y. H. Lin, *ACS nano.*, 2010, **4**, 1790-1798.
31 P. Si, S. Ding, J. Yuan, X. W. Lou and D.-H. Kim, *ACS nano.*, 2011, **5**, 7617-7626.
32 Q. Y. Yan, B. Peng, G. Su, B. E. Cohan, T. C. Major and M. E. Meyerhoff, *Anal. Chem.*, 2011, **83**, 8341-8346.